Neuron, Vol. 38, 103–114, April 10, 2003, Copyright ©2003 by Cell Press

Receptive Fields of Disparity-Tuned Simple Cells in Macaque V1

Doris Y. Tsao,* Bevil R. Conway, and Margaret S. Livingstone
Department Neurobiology
Harvard Medical School
220 Longwood Avenue
Boston, Massachusetts 02115

Summary

Binocular simple cells in primary visual cortex (V1) are the first cells along the mammalian visual pathway to receive input from both eyes. Two models of how binocular simple cells could extract disparity information have been put forward. The phase-shift model proposes that the receptive fields in the two eyes have different subunit organizations, while the position-shift model proposes that they have different overall locations. In five fixating macaque monkeys, we recorded from 30 disparity-tuned simple cells that showed selectivity to the disparity in a random dot stereogram. High-resolution maps of the left and right eye receptive fields indicated that both phase and position shifts were common. Single cells usually showed a combination of the two, and the optimum disparity was best correlated with the sum of receptive field phase and position shift.

Introduction

Stereopsis is the ability to perceive depth from binocular disparity, or the difference between the images in the two eyes. It is likely that stereoscopic depth processing starts in V1, since this is the first site in the primate visual system where disparity-tuned cells have been found (Pettigrew, 1965; Barlow et al., 1967; Poggio and Fischer, 1977). Furthermore, it is likely that stereoscopic depth processing in V1 starts in binocular simple cells, because (1) disparity tuning in complex cells is often much narrower than the receptive field width, and (2) complex cells invert their disparity tuning to opposite contrast bars, i.e., disparities which are excitatory become inhibitory and vice versa (Ohzawa et al., 1990; Cumming and Parker, 1997; Livingstone and Tsao, 1999). The inversion implies that the stage at which disparity selectivity is generated must give opposite responses to opposite contrast stimuli; this is true of geniculate cells and simple cells, but not of complex cells.

A fundamental question concerning disparity-tuned simple cells is whether the disparity selectivity is generated by differences between the two eyes' receptive field locations (position-shift model) or by differences in receptive field organization (phase-shift model) (Figure 1A) (for review, see Qian, 1997). The position-shift model is intuitively simple to understand: disparity, which is due to a horizontal shift between the left and right eye images, is computed by a cell with a horizontal shift between the two eyes' receptive fields. The phase-shift model proposes that disparity is computed by a difference in the arrangement of ON and OFF subunits between the two eyes' receptive fields. This model is based on the hypothesis that simple cell receptive fields are well modeled by Gabor functions (Marcelja, 1980; Daugman, 1985; Jones and Palmer, 1987). A Gabor function is a product of a Gaussian and a sine wave. The phase of a Gabor refers to the phase of the sine wave and represents a way to describe the sequence of ON and OFF subunits. The position-shift model can also be represented in terms of a Gabor model, as a shift in the center location of the Gaussian.

The shape of the disparity tuning curve of a binocular simple cell is determined by whether its monocular receptive fields are related through a phase or a position shift, assuming the inputs to the cell interact multiplicatively (see Supplemental Appendix 1 at http://www.neuron.org/cgi/content/full/38/1/103/DC1). Position shifts produce *symmetric* disparity tuning curves (Figure 1B), while phase shifts produce *asymmetric* disparity tuning curves. If one assumes that simple-cell disparity tuning curves are inherited by downstream complex cells, then measurements of disparity tuning in complex cells (which are numerous in the monkey) can be used as an indirect assay for the underlying mechanism used in simple cells. Applying this method, Prince et al. (2002a) inferred that both phase and position shifts are common in the monkey. But given that (1) the shape of the disparity-tuning curve of a complex cell is most likely a result not only of the shape of disparity tuning in underlying simple cells, but also of interactions between complex cells, and (2) a complex cell integrates the outputs of multiple simple cells, which may or may not all use the same mechanism to generate disparity selectivity, it is risky to extrapolate simple-cell subunit organization from complex cell disparity-tuning curves.

Direct comparisons of monocular receptive fields have all been made in the anesthetized cat. Hubel and Wiesel (1962) and Maske et al. (1984) mapped monocular receptive field profiles of binocular simple cells in the anesthetized cat with moving light and dark bars and found that the number and sequence of ON and OFF subunits were the same in the two eyes, supporting the position shift model. But they did not examine differences in the relative strength of the subunits in the two eyes, which could also generate phase shifts. By mapping left and right eye receptive fields of simple cells, Freeman and coworkers have shown clearly that phase is a parameter that can differ between the two eyes (DeAngelis et al., 1991; Ohzawa et al., 1996; Anzai et al., 1999a). However, because they worked in anesthetized animals, in which the relative position of the eyes is unknown, the relationship between phase differences and disparity tuning (if any) could not be resolved.

Since the output of disparity-tuned simple cells likely constitutes the building blocks for all later disparity computations, which ultimately lead to the percept of 3D depth, it is important to understand precisely how these cells integrate information from the two eyes. In this

*Correspondence: doris@nmr.mgh.harvard.edu

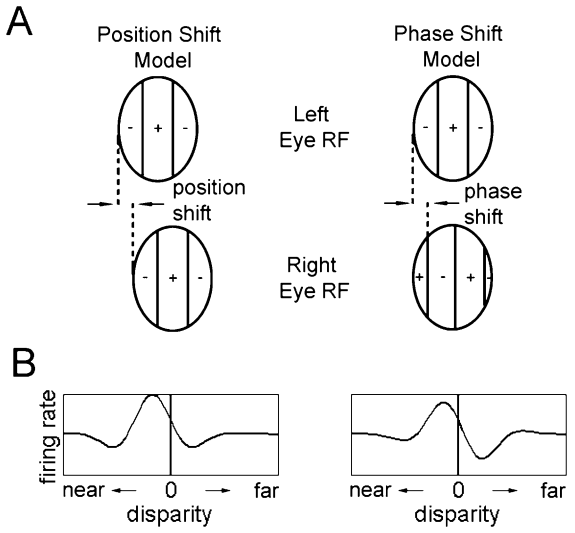

Figure 1. Position-Shift versus Phase-Shift Models for Generating Disparity-Tuned Simple Cells

(A) Adapted from Figure 3 in Qian (1997). In the position-shift model, the left and right eye receptive fields have the same phase, but different horizontal positions. In the phase-shift model, the left and right eye receptive fields are in the same position, but differ in phase. (B) The disparity-tuning curves predicted by the position-shift model (left) and phase-shift model (right) assuming that inputs from the two eyes interact multiplicatively. The position-shift model predicts symmetric disparity-tuning curves, while the phase-shift model predicts asymmetric disparity-tuning curves.

study, we measured left and right eye receptive field maps in five alert, fixating macaques in which eye position was known and disparity tuning could be measured. We found that both phase and position differences contribute to the shape of the disparity-tuning curve in binocular simple cells of the macaque.

Results

We obtained monocular receptive field maps and binocular interaction maps from 30 simple cells. Twelve were tuned for near disparities, ten for far, four for zero, and four were tuned inhibitory, with a trough near zero disparity.

In four monkeys, we initially screened for disparity-selective cells using a dynamic random-dot stereogram. Out of 794 cells screened, we found 172 disparity-tuned cells, of which 154 were complex and 18 were simple. Because simple cells appear to be relatively rare and this study concerns them specifically, in a fifth monkey we subsequently screened cells for simple structure (Conway and Livingstone, 2002). This method of screening yielded 16 simple cells of which 12 were disparity selective and included in our analysis, to give a total population of 30 disparity-tuned simple cells.

Screening for Disparity-Tuned Simple Cells

We used a dynamic random dot stereogram (Julesz, 1960) to test for disparity selectivity, in order to eliminate any monocular cues to depth. The stereogram consisted of a central square region which alternated between a near ($-0.14°$) and a far ($0.09°$) disparity, and a surrounding region which was held at a fixed far ($0.09°$) disparity. The size of the central region covered the receptive field of the cell. We classified a cell as disparity tuned if it clearly responded differently to the two disparities.

After a disparity-tuned cell was isolated, we mapped each eye's receptive field along one dimension. We used pairs of light bars to map the ON subregions in the two eyes, and pairs of dark bars to map the OFF subregions in the two eyes. To plot the "spacetime map," we computed the average poststimulus time histogram (PSTH), from 0 to 250 ms, to stimulation at each bar location (see Figure 8 for a quantification of the stability of the spacetime maps). Figure 2A shows, for one simple cell, the left and right eye spacetime maps in response to light bars (top row) and dark bars (bottom row). The light-bar response was spatially and temporally offset from the dark-bar response, in both eyes. In each spacetime map, the horizontal axis represents the location of the stimulus, the vertical axis represents the time after stimulus presentation, and the average firing rate is plotted, in spikes/s, according to the colorscale. The reason for the horizontal striations (which occur every 17 ms) in the dark bar spacetime plot is that the cell responded to the background at the refresh rate of the monitor (60 Hz).

From the spacetime maps, we extracted one-dimensional spatial and temporal response profiles (white lines in Figure 2A). We fit the spatial and temporal response profiles from both light- and dark-bar maps to sinusoids and classified a cell as simple when the light and dark response profiles were more than $90°$ out of phase either spatially or temporally. Figure 2C shows a scatter plot of the temporal versus spatial phase differences between light and dark maps for our entire population of disparity-tuned cells. The simple cells are all scattered in the upper right quadrant (light and dark maps $>90°$ out of phase both spatially and temporally), while the complex cells are clustered in the lower left quadrant (light and dark bar maps $<90°$ out of phase both spatially and temporally). We used the light- and dark-bar spacetime maps from the dominant eye to compute the phase differences shown in this plot. This is valid because most cells were either simple in both eyes or complex in both eyes. There were two cells that were exceptions; these cells responded to only a single contrast in each eye (Figure 2B). For these cells (denoted by an asterisk in Figure 2C), the temporal and spatial phase differences were computed using the light-bar map in one eye and the dark-bar map in the other eye. Both cells responded to the random dot screening stimulus, showing that they were disparity tuned.

Relationship between Monocular Left and Right Eye Receptive Fields: Phase Shift or Position Shift?

Figures 3 and 4 demonstrate how we measured the disparity tuning and compared this to the monocular receptive fields for the cell in Figure 2A. In response to the screening random dot stereogram, this cell responded preferentially to a near compared to a far disparity (Figure 3A). We confirmed that the cell was near by plotting its disparity-tuning curve to a changing-disparity binocular bar that was moved back and forth

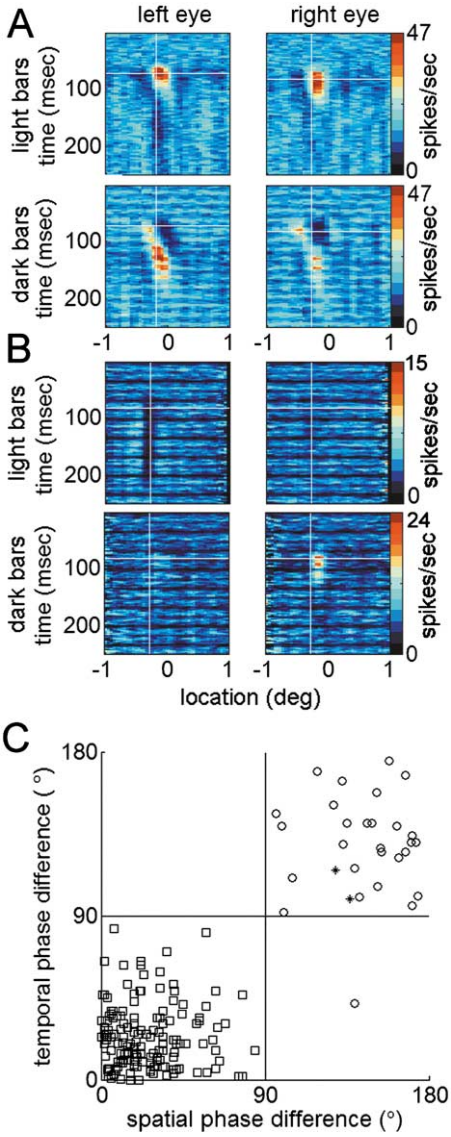

Figure 2. Classifying Cells as Simple

(A) Top row: left and right eye spacetime maps of a disparity-tuned simple cell mapped with light bars. Bottom row: left and right eye spacetime maps of the same cell mapped with dark bars. The light- and dark-bar responses were spatially and temporally complementary.

(B) Light- and dark-bar monocular spacetime maps for a cell sensitive to only a single contrast in each eye.

(C) Scatter plot of temporal versus spatial phase shift for the 30 binocular simple cells (open circles, asterisks), compared to 154 disparity-tuned complex cells (open squares). For the two simple cells marked with an asterisk, phase differences were computed across eyes.

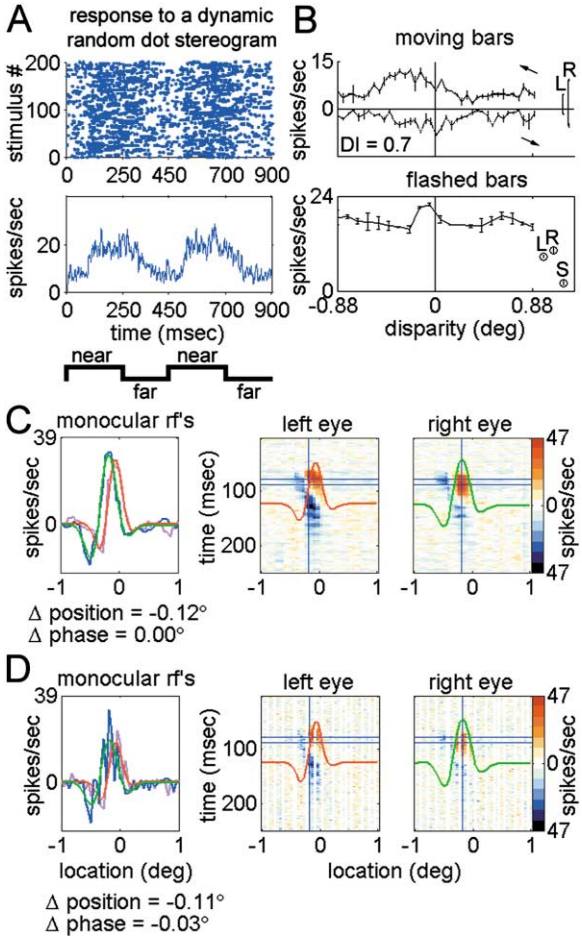

Figure 3. A Position-Shifted Near Simple Cell

This is the same cell whose light- and dark-bar response maps are shown in Figures 2B and 2C.

(A) A raster plot showing that the cell responded preferentially to a near random dot stereogram.

(B) The disparity-tuning curve to a disparity bar moving in opposite directions (top), as well as to a flashed bar (bottom). For both moving and flashed bars, the left and right eye monocular responses are shown. The spontaneous firing rate is also shown for flashed bars. The peak of the flashed bar disparity-tuning curve was $-0.10°$.

(C) First column: the receptive-field profile in the left and right eyes fitted to a Gabor function (red, left eye Gabor fit; green, right eye Gabor fit; magenta, left eye raw data; blue, right eye raw data). Second and third columns: left and right eye spacetime maps. The *x* axis represents the stimulus location, and the *y* axis represents the time following the stimulus presentation. The colorscale is calibrated symmetrically about zero; red regions represent excitation to light bars, and blue regions represent excitation to dark bars. The two horizontal lines in each map mark the 10 ms time interval over which the average receptive field profile was computed. The monocular receptive field profiles are also shown superimposed on both spacetime maps. This cell had a position shift of $-0.12°$ and a phase shift of $0.00°$. Both spacetime maps have been filtered with a pseudo-Gaussian 3×3 matrix with sigma $= 0.14°$ in space and 3 ms in time.

(D) The same set of maps as for (C), without filtering.

(Figure 3B, top), as well as flashed at random locations within the receptive field (Figure 3B, bottom). The second disparity-tuning curve was calculated from the binocular two-bar interaction map by summing along iso-disparity diagonals (see Experimental Procedures for details).

The left and right eye spacetime maps of this cell are shown in Figure 3C, second and third columns. They were computed by subtracting, for each eye, the dark-bar spacetime map (Figure 2A, bottom row) from the light-bar spacetime map (Figure 2A, top row). This subtraction makes the assumption that wherever a simple

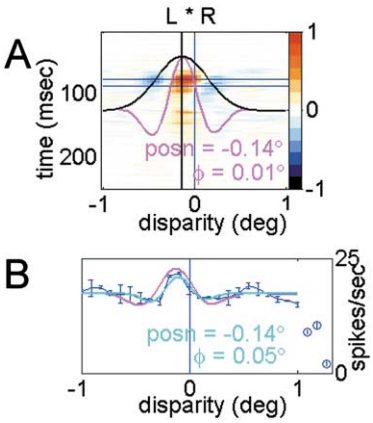

Figure 4. The Cross-Correlogram Method Is a Simpler Way to Compute Interocular Phase and Position Shift

(A) The cross-correlation of the left and right eye spacetime maps for the cell in Figure 3, scaled to an amplitude of 2. Superimposed is a cross-correlation profile (magenta curve), averaged over the temporal range indicated by the blue horizontal lines. The Gaussian envelope of the cross-correlation profile is shown in black, and the center of the Gaussian is indicated by a black vertical line. The interocular cross-correlogram of this cell had a position of −0.15° and a phase of 0.05°.

(B) The actual disparity-tuning curve (blue, raw data; cyan, Gabor fit). The predicted disparity-tuning curve (magenta) is redrawn from (A), with rescaling.

cell is excited by a light bar, it is inhibited by a dark bar, and vice versa (Movshon et al., 1978). Since inhibitory synaptic potentials below a cell's firing threshold will be masked, the full strength of ON and OFF subregions can only be revealed by subtracting dark-bar responses from light-bar responses. Three features are apparent in the monocular spacetime maps: (1) the sequence of ON and OFF subunits is the same in the two eyes; (2) the left eye receptive field is shifted to the right of the right eye receptive field; and (3) there is a slant to the receptive field such that it shifts leftward with shorter delay. The crossed receptive field shift was consistent with the cell's near disparity preference, and the leftward slant of the monocular receptive fields was consistent with the cell's leftward motion preference (McLean and Palmer, 1989; Reid et al., 1991; DeAngelis 1993a, 1993b; Ohzawa et al., 1996; Conway and Livingstone, 2002).

To determine the precise combination of phase- and/or position-shift between the two eyes, we fit the monocular receptive field profiles to Gabor functions. The receptive field profiles were obtained by averaging the spacetime maps over a range centered about the optimum delay (indicated by the pair of horizontal blue lines in Figure 3C, second and third columns). The resulting monocular receptive field profiles are shown in the left column of Figure 3C (magenta, left eye; blue, right eye). Using the Levenberg-Marquardt algorithm (Press et al., 1992), we fit the receptive field profile in each eye to a Gabor function, allowing the spatial frequency, phase, center, amplitude, vertical offset, and sigma of the Gabor to vary. The resulting Gabor fits are shown in Figure 3C, superimposed on the monocular spacetime maps and on the raw receptive field profile traces. To compare the magnitude of phase versus position shift, we converted the phase difference between the two Gabors to an equivalent disparity by dividing by the spatial frequency of the Gabor (averaged over the two eyes). This cell had a position shift of −0.12° and a phase shift of 0.00° (we use the convention that near disparities are negative). The actual optimal disparity of the cell, measured with a flashing disparity bar, was −0.10° (Figure 3B), in good agreement with the interocular position shift.

The monocular spacetime maps in Figure 3C were filtered with a 3 × 3 pseudo-Gaussian filter, sigma 0.14° in the spatial dimension and 3 ms in the time dimension. This smoothed the maps without significantly altering their organization. Figure 3D shows the monocular spacetime maps without filtering. When phase and position disparities are calculated from the unblurred maps, position disparity is still greater than phase disparity.

We fit the left and right eye receptive field profiles of all 30 simple cells to Gabor functions. With a few exceptions, the fits described the data quite well; on average, they accounted for 91% of the variance in the data. However, it is dangerous to directly use the parameters of the Gabor fits to assess the contributions of phase and position, because the parameters may not be well constrained. If a different set of phase and position values could yield an equally good fit, this obviously presents a problem. Furthermore, for receptive fields with a single subunit, a Gabor may not even be necessary; a Gaussian may be sufficient. In order to assess: (1) whether a Gabor function was necessary, and (2) when a Gabor was necessary, how well constrained the phase and position parameters of the Gabor were, we applied the sequential F test method (Draper and Smith, 1998). For each cell, we fit the left and right eye receptive fields to the following four curves: (1) a Gabor with phase and position parameters allowed to vary freely, (2) a Gaussian, (3) a Gabor with the phase parameter free but with the position parameter constrained to be the same in both eyes, and (4) a Gabor with the position parameter free but with the phase parameter constrained to be the same in both eyes. We then compared fits 2, 3, and 4 with fit 1, using the sequential F test, to determine whether they yielded equally good fits or not (see Experimental Procedures for details).

When we applied this fitting procedure to all the cells, we found that for 6/30 cells, the results were ambiguous: in at least one eye, a phase-constrained Gabor and a position-constrained Gabor were both able to fit the data just as well as a full, unconstrained Gabor (see Supplemental Figure S1 at http://www.neuron.org/cgi/content/full/38/1/103/DC1). This was due to the high number of degrees of freedom in the fitting procedure (12 for the unconstrained Gabor fits, 11 for the constrained Gabor fits) and the fact that a phase shift can be partially compensated by differences in other parameters, e.g., relative spatial frequency, receptive field width, and amplitude.

Thus we needed to adopt an approach for computing receptive field phase and position shifts that involved fewer degrees of freedom. The half-squaring model actually makes a very specific prediction about the shape of a cell's disparity-tuning curve, given its monocular receptive field profiles. It predicts that the disparity-tuning curve should equal the *cross-correlogram* of the monocular receptive field profiles. For a binocular sim-

ple cell with Gabor-shaped monocular receptive fields, the disparity-tuning curve should also be a Gabor function, with phase equal to the *phase shift* between the monocular receptive fields and position equal to the *position shift* between the monocular receptive fields (for proof, see Supplemental Appendix 1 at http://www.neuron.org/cgi/content/full/38/1/103/DC1). To avert the ambiguities associated with extracting parameter differences between two independently fit curves, we decided a better approach would be to extract phase and position disparities by fitting a Gabor function to the interocular cross-correlogram, a single curve.

Figure 4A shows the cross-correlation of the monocular spacetime maps for the position-shift cell in Figure 3. The Gabor fit to the one-dimensional cross-correlation profile is superimposed (magenta curve). This represents the disparity-tuning curve predicted by the half-squaring model. Also shown is the position envelope of the cross-correlation profile. It is easy to read off the phase and position shift from such a cross-correlation plot: the position shift is equal to the horizontal displacement of the black line (marking the center of the position envelope) from the blue line (marking zero disparity), while the phase shift is equal to the horizontal displacement of the peak of the magenta curve from the black line. For this cell, the half-squaring model yields a predicted $\Delta\text{posn} = -0.14^\circ$ and $\Delta\text{phase} = 0.01^\circ$. These two values are in good agreement with the values obtained by fitting monocular receptive fields (Figure 3C). They are also in good agreement with the phase and position values of the actual disparity-tuning curve ($\Delta\text{posn} = -0.10^\circ$ and $\Delta\text{phase} = 0.01^\circ$). Figure 4B shows the actual disparity-tuning curve (blue curve, raw data; cyan curve, Gabor fit) obtained by summing along iso-disparity diagonals of the binocular two-bar interaction map, together with the predicted disparity-tuning curve (magenta curve).

Figure 5 presents results from nine more disparity-tuned simple cells that had various combinations of phase and/or position shifts between the two eyes. For each cell, the first column shows the left and right eye receptive field profiles, the second and third columns show the left and right eye spacetime maps with receptive field profiles superimposed, the fourth column shows the cross-correlation of the left and right eye spacetime maps together with the predicted disparity-tuning curve, and the fifth column shows the actual disparity-tuning curve together with the predicted disparity-tuning curve.

Figure 5A shows a near cell whose left and right eye receptive fields were related mainly through a position shift. This is reflected in the symmetry of the predicted disparity-tuning curve. Figures 5B–5D show three more near cells whose left and right eye receptive fields were related mainly through a phase shift. The predicted disparity-tuning curves of these three cells were asymmetric, while the envelope position was close to zero. Figures 5E and 5F shows two hybrid phase- and position-shift cells in which the predicted phase and position disparity were in the same direction (Figure 5E, both near; Figure 5F, both far). Figure 5G shows a third hybrid phase- and position-shift cell, in which the predicted phase and position disparities were in opposite directions (near phase shift, far position shift). The actual disparity-tuning curve of this cell, however, was symmetric. Figures 5H and 5I show two tuned inhibitory cells. The monocular receptive fields of these cells were monophasic, and the ON region in one eye was in the same location as the OFF region in the other eye. Both of these cells responded only to light bars in the left eye and dark bars in the right eye. The actual disparity-tuning curves for both cells showed a trough at zero disparity.

The examples in Figures 3, 4, and 5 demonstrate that for different simple cells, disparity selectivity can be generated by phase, position, or a combination of the two. Indeed, when we assessed the significance of the phase and position parameters of the Gabor fits to the predicted disparity-tuning curves (using the sequential F test method), we found that, except for the four tuned inhibitory cells and two tuned excitatory cells, a nonzero phase and position were both required, supporting the hybrid phase- and position-shift model.

Figure 6 presents the results from our entire population of 30 cells. Figure 6A shows a scatter plot of the phase of the predicted disparity-tuning curve versus the phase of the actual disparity-tuning curve, both in degrees phase angle. Angular correlation coefficient $r = 0.56$ (significant, Upton and Fingleton test; Zar, 1999, page 651). Figure 6B shows a scatter plot of the position of the predicted disparity-tuning curve versus the position of the actual disparity-tuning curve ($r = 0.67$, $p < 2 \times 10^{-5}$). Thus both the phase and the position of the actual disparity-tuning curve were significantly correlated with the values predicted by the half-squaring model.

One would therefore expect that the peak of the actual disparity-tuning curve should be best correlated with the sum of receptive field phase and position shift. Figures 6C–6F show that this is indeed the case. Figure 6C plots predicted phase against the peak of the actual disparity-tuning curve, and Figure 6D plots predicted position against actual peak disparity (in degrees visual angle). The phase disparity in visual angle of the four tuned inhibitory cells was taken as zero (but the phase disparity in phase angle was taken as 180°), since this was the position of maximum binocular interaction (Prince et al., 2002a). The predicted position was significantly correlated to the actual peak ($r = 0.74$, $p < 1.6 \times 10^{-6}$), but the predicted phase was not ($r = 0.28$, $p < 0.06$). Figure 6E plots the sum of predicted phase and position shifts against the actual peak. This resulted in a better correlation than either position or phase alone ($r = 0.82$, $p < 2.0 \times 10^{-8}$), supporting the hybrid phase- and position-shift model. The sum of the phase and position of a Gabor function can overestimate the peak of the Gabor if the period of the Gabor is much larger than its width. Therefore, the peak of the Gabor is a better way to express the combined effect of the phase and position of the Gabor. Figure 6F plots the peak of the predicted disparity-tuning curve against the peak of the actual disparity-tuning curve. As expected, this produces a slight improvement in the correlation ($r = 0.91$, $p < 2.3 \times 10^{-12}$). Together, Figures 6C–6E demonstrate that a hybrid phase/position-shift model best explains the generation of disparity tuning in binocular simple cells.

Figure 7A presents a scatter plot of predicted phase versus position shifts, together with histograms of

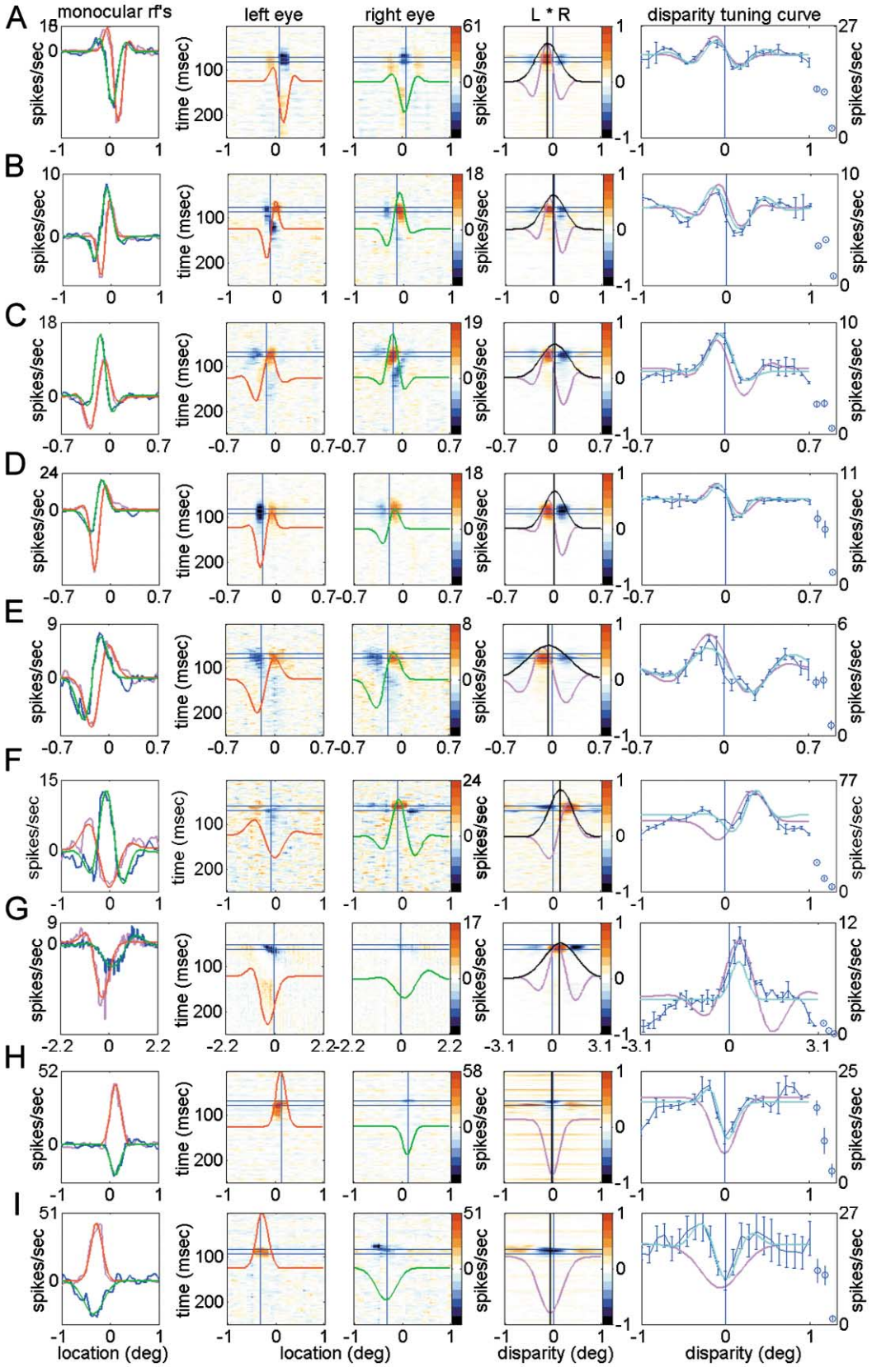

Figure 5. Spacetime Maps and Interocular Cross-Correlation Functions for Nine Disparity-Tuned Simple Cells Reveal that Various Combinations of Phase and Position Shifts Exist between the Two Eyes' Receptive Fields

The first column shows the monocular receptive field profiles, the second and third columns show the left and right eye spacetime maps with

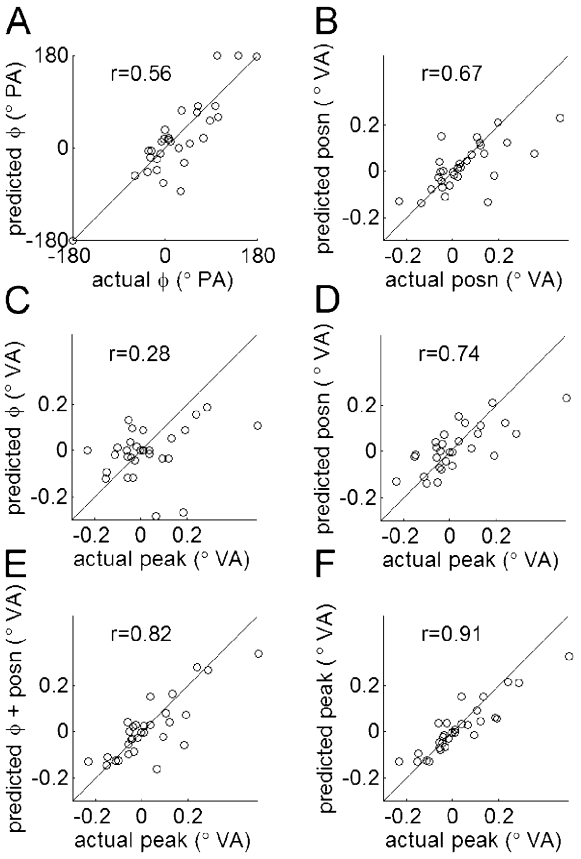

Figure 6. Disparity Selectivity Is Generated by Both Position and Phase

(A) A scatter plot of the RF phase shift (computed from the cross-correlogram of the two eyes' receptive field profiles) versus the phase of the actual disparity-tuning curve, both in degrees phase angle. Angular correlation coefficient r = 0.67.

(B) RF position shift versus the position of the actual disparity-tuning curve.

(C) RF phase shift versus the peak of the actual disparity-tuning curve.

(D) RF position shift versus the peak of the actual disparity-tuning curve.

(E) Sum of RF phase and position shifts versus the peak of the actual disparity-tuning curve.

(F) Peak of the predicted disparity-tuning curve versus peak of the actual disparity-tuning curve. n = 29 for all plots. The cell in Figure 5G is not shown because its phase and position shifts were too large (phase shift = −0.42°, position shift = 0.73°).

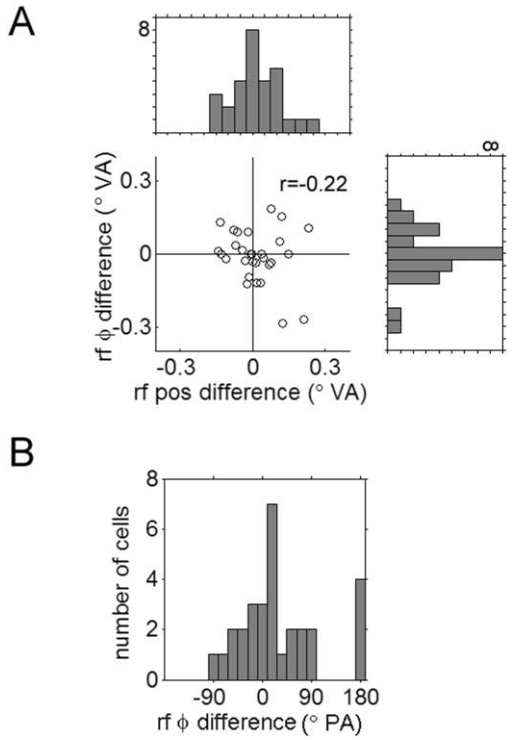

Figure 7. Distribution of RF Phase and Position Shifts

(A) Scatter plot of phase disparity versus position disparity (both in degrees visual angle), and histograms for each. The two types of disparity spanned similar ranges. There was an insignificant negative correlation between the two (r = −0.22, p < 0.1).

(B) Histogram of phase in degrees phase angle. All cells have a phase angle disparity of <90°, except for the four tuned inhibitory cells.

phase- and position-shift values. The magnitudes of the two parameters were similar (average position disparity = 0.24°, average phase disparity = 0.20°) and showed a negative correlation to each other, which did not reach significance (r = −0.22, p < 0.1).

Classes of Disparity-Tuned Cells

Disparity-tuned cells have been classified into six categories: near, far, tuned near, tuned far, tuned zero, and tuned inhibitory (Poggio and Fischer, 1977; Poggio et al., 1988, 1990). Translated into the language of phase and position shifts, tuned zero, near, and far neurons

receptive field profiles superimposed, the fourth column shows the cross-correlation of the left and right eye spacetime maps together with the predicted disparity-tuning curve, and the fifth column shows the actual disparity-tuning curve together with the predicted disparity-tuning curve.

(A) A near cell whose left and right eye receptive fields were related mainly through a position shift. The predicted disparity-tuning curve (magenta) for this cell was symmetric.

(B–D) Three more near cells whose left and right eye receptive fields were related mainly through a phase shift. The predicted disparity-tuning curve (magenta) for these cells was asymmetric, and the envelope position was close to zero.

(E and F) Two hybrid phase- and position-shift cells in which phase and position disparity were in the same direction (both near for [E], both far for [F]).

(G) Another hybrid phase- and position-shift cell (mapped at 11.6° eccentricity), in which phase and position disparities were in opposite directions (near phase shift, far position shift). The actual disparity-tuning curve of this cell was symmetric.

(H and I). Two tuned inhibitory cells. The monocular receptive fields of these cells were monophasic. The actual disparity-tuning curves showed a trough at zero disparity.

have 0° phase shift, near and far neurons have ±90° phase shift, and tuned inhibitory neurons have 180° phase shift between the left and right eye receptive fields. In the current study we found a continuum of phases between −90° and 90° (Figure 7B). Thus, in agreement with Prince et al. (2002a), we conclude that tuned excitatory, tuned near, tuned far, near, and far neurons do not form distinct classes of cells. However, phase shifts were not distributed evenly between 0° and 180°, but were less than 90° for all except the four tuned inhibitory cells, which had a phase difference of 180° (Rayleigh's R test for circular uniformity, $p < 3.6 \times 10^{-4}$). The overwhelming concentration of neurons with phase less than 90° is also evident in the data of Prince et al. (2002a) and Anzai et al. (1999a). Thus it is possible that tuned inhibitory neurons constitute a separate class of cells.

Conjugate and Vergence Eye Movements

The advantage of using alert animals to study stereopsis is that the actual disparity preference and the actual position shift between the left and right eye receptive fields can be measured because the monkey can be trained to fixate. However, there may be doubt whether receptive field mapping in alert monkeys has the necessary resolution, since the animal is free to move its eyes (though it is rewarded for fixating). In theory, it would be optimal to correct the bar position for the position of each eye so that the receptive field maps represent the position of the bar on the monkey's retina rather than the position on the screen (Livingstone, 1998; Livingstone and Tsao, 1999; Conway, 2001; but see B.G. Cumming and J.C.A. Read, 2002, Soc. Neurosci., abstract). When we did this for all the cells studied here, we found that eye position correction improved resolution in some cells and did not in others. The benefit of eye position correction appears to depend on how well the monkey fixates. On average, eye position correction resulted in receptive field profiles with slightly smaller amplitudes (mean ratio = 0.95 ± 0.27) and larger widths (mean ratio = 1.16 ± 0.30) (see Supplemental Figure S2 at http://www.neuron.org/cgi/content/full/38/1/103/DC1). Despite this, we obtained similar results using eye position-corrected and non-eye position corrected maps. For consistency, all of the maps and analysis shown here were done on non-eye position corrected maps (with the exception of Supplemental Figure S2 at http://www.neuron.org/cgi/content/full/38/1/103/DC1).

Uncorrected conjugate eye movements would blur receptive fields and drive small phase shifts toward zero (by making the receptive fields monophasic), but would leave position shifts unchanged. During the present recordings, the average standard deviation of the eye position was 0.07° (computed across time within a typical trial in which light- and dark-bar receptive field maps were obtained for both eyes). It is likely that these values are larger than the magnitude of actual microsaccades, since receptive field blurring was evident with the use of eye position correction.

Vergence eye movements could distort the measurements of both phase and position shifts. The standard deviation of "vergence error" (i.e., the difference between the two eye's positions) was 0.08°. We believe this vergence error represents an instrumental limitation, and our monkeys actually maintained vergence much more accurately than this, because the phase and position shift measurements were repeatable. For all 30 cells, for both light- and dark-bar maps, we divided the total number of spikes into two blocks, block A and block B, and computed spacetime maps from the spikes in block A and block B separately. Block A consisted of the first half of the light- and dark-bar spikes, and block B consisted of the second half of the two sets of spikes. Thus, for each cell we had two independent estimates of the left and right eye receptive field profiles. Figure 8 shows the results of this analysis. Figure 8A shows the

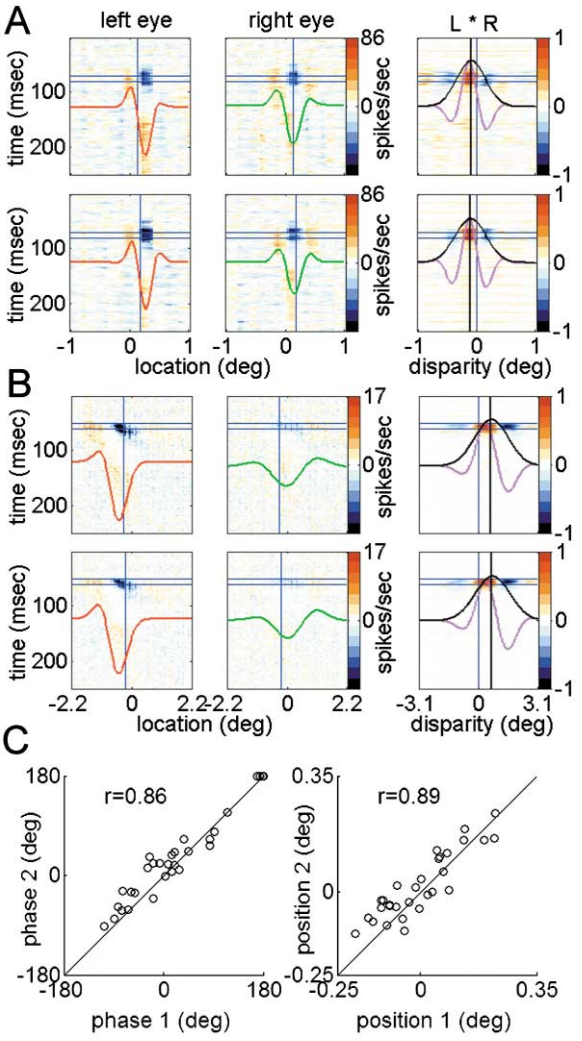

Figure 8. Repeatability of Predicted Phase and Position Parameters

(A) Repeated monocular spacetime maps and interocular cross-correlation maps for the cell in Figure 5A. The two sets of maps (top and bottom) were generated from two independent sets of spikes. The cross-correlation of the left and right eye maps is shown in the far right column. Note the stability of the phase and position of the predicted disparity-tuning curve.

(B) Repeated spacetime maps and cross-correlation functions for the cell in Figure 5G.

(C) Scatter plots of the phase (left) and envelope position (right) of the interocular cross-correlogram, computed off spikes in block A versus spikes in block B (see text for details).

repeated monocular spacetime maps and interocular cross-correlation map for the cell in Figure 5A. The phase and position parameters remained constant. Figure 8B shows another example (same cell as Figure 5G). Figure 8C shows a scatter plot, across the entire population, of the phase and position parameters obtained from the two independent sets of left and right eye spacetime maps. The correlation for phase was $r = 0.86$, and for position it was $r = 0.89$. Thus the phase and position shift measurements were stable.

Discussion

How are the inputs from the two eyes first combined in generating stereopsis? Because disparity tuning in complex cells inverts to anticorrelated stimuli, we know that disparity selectivity arises in simple cells or in simple-cell-like dendritic compartments. The main finding of this study is that in alert macaque V1, disparity-selective simple cells generate disparity tuning by a combination of phase and position shift, as in binocular simple cells in the anesthetized cat (Anzai et al., 1999a).

The ratio of simple to complex disparity-selective cells (0.10) seems rather low for simple cells to be the source of disparity selectivity in complex cells, but it is not impossible since different complex cells could be receiving input from the same simple cell. Alternatively, the ratio may be due to an electrode sampling bias. Most of the simple cells we recorded from for this study were sparsely firing cells in layer 4B and in the upper layers (based on electrode penetration distance relative to layer 4C).

There has been some debate about whether simple cells are capable of computing the disparity in random dot stereograms (Poggio, 1984). Anzai et al. (1999b) suggested that since the response of simple cells to a dynamic random dot stereogram depends on the monocular phase of the stimulus, the response would be sporadic and difficult to associate with the disparity of the stereogram. Here, we found that disparity-tuned simple cells responded in a robust, disparity-specific manner to dynamic random dot stereograms. Furthermore, the precise shape of the disparity-tuning curve matched the prediction of the half-squaring model (Anzai et al., 1999b). Half-squaring could be implemented by a simple threshold mechanism. Anderson et al. (2000) have pointed out that the membrane potential is not constant but fluctuates due to noise. Thus, over time, thresholding can approximate a half-squaring function.

Many of the disparity-tuned simple cells were also direction selective. The co-wiring of disparity and direction in these cells could underlie the Pulfrich phenomenon, the ability to perceive depth through pure temporal disparities (Qian and Andersen, 1997; Anzai et al., 2001). The Pulfrich phenomenon is ecologically important because it allows detection of the depth of monocularly-occluded moving features, which occur whenever there is motion behind an edge with a vertical component (Burr and Ross, 1979; Shimojo et al., 1988).

Why Might the Visual System Use Both Position and Phase Disparities?

There are two distinct forms of stereopsis, one for perceiving the depth of features visible to both eyes (Wheatstone stereopsis) and another for perceiving the depth of features occluded in one eye by a foreground object (da Vinci stereopsis) (Nakayama and Shimojo, 1990; Anderson and Nakayama, 1994). Inquiries into the neural mechanisms of stereopsis have focused almost exclusively on the former. Yet the visual system clearly uses binocular occlusion geometry to recover depth. This is demonstrated by Figure 9A, which shows two "da Vinci stereograms" that elicit different depth percepts, even though neither stereogram contains any correlated nonzero disparities. Rather, the only cues to the depth of the black flanks are from occlusion. In stereogram 1 (Figure 9A, top) the flanks appear at a far depth, while in stereogram 2 (Figure 9A, bottom) they appear at zero disparity, behind an illusory rectangular near window. The physical situation which would give rise to each stereogram is diagrammed to the right of Figure 9A.

We suggest that the visual system employs a hybrid of phase and position shifts in order to deal with da Vinci stereopsis. Figure 9B, left, shows a magnified view of the stimulus geometry at the left edge of stereogram 1, together with the interocular image correlation profile computed from the magnified view. This correlation pro-

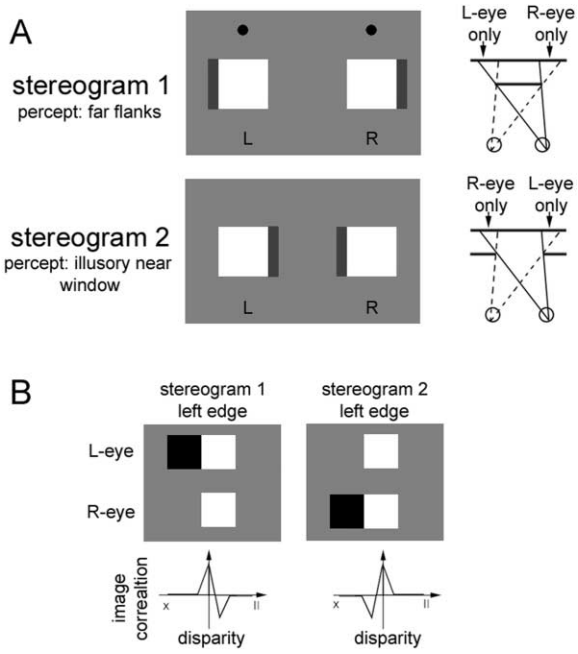

Figure 9. Da Vinci Stereopsis Generates Interocular Image Correlation Profiles with Both Phase and Position Shifts

(A) Two da Vinci stereograms. Divergent fusion of the top stereogram reveals a zero disparity square with two black flanks at a far depth. Divergent fusion of the bottom stereogram reveals a zero disparity square behind a near illusory window. Crossed fusion switches the percepts generated by the two stereograms. The diagrams on the right depict the physical situations that could give rise each stereogram. For example, stereogram 1 could be generated by viewing a white square in front of a black wall.

(B) Magnified views of the left edge of stereograms 1 and 2, together with the interocular image correlation profiles computed from the magnified views. The left edge of stereogram 1 contains a crossed phase shift and an uncrossed position shift. The left edge of stereogram 2 contains an uncrossed phase shift and a crossed position shift.

file contains a hybrid of an uncrossed position shift and a crossed phase shift. The correlation profile for stereogram 2 (Figure 9B, right) also contains a hybrid of position and phase shifts, but in a different combination: a crossed position shift and an uncrossed phase shift. To distinguish between these two stereograms, i.e., to accomplish da Vinci stereopsis, a population of hybrid phase- and position-shifted simple cells would be helpful. Position-shifted cells alone would be insufficient because they are only sensitive to absolute peak or trough locations, and not to asymmetric relationships between the two (though the latter could be accomplished by pooling the outputs of tuned excitatory and tuned inhibitory cells in asymmetric combinations at a subsequent stage). Phase-shifted cells alone would also be insufficient, because da Vinci stereopsis would then be limited to a single occluding depth plane. Wheatstone stereopsis, in contrast, can be carried out by either phase- or position-shifted cells (Qian, 1997).

The natural world is rich in occlusion configurations—fruit hanging behind leaves and branches, etc.—and thus often generates asymmetric interocular correlations. Hybrid phase- and position-shifted simple cells may develop through Hebbian mechanisms driven to replicate the interocular correlation statistics of natural stereo images.

Experimental Procedures

Recordings

Recording techniques and reverse-correlation mapping with correction for eye position have been described (Livingstone, 1998; Livingstone and Tsao, 1999; Conway, 2001). Briefly, five male rhesus macaque monkeys were implanted with head posts, recording chambers, and eye coils under sterile conditions. Eye coils were sutured to the sclera with four sutures, 90° apart. The chambers were centered over the lateral operculum, allowing access to foveal V1.

We recorded extracellularly with fine electropolished tungsten electrodes coated with vinyl lacquer (Frederick Haer, Bowdoinham, ME). Extracellular signals were amplified, bandpass filtered (500Hz–2 kHz), and fed into a dual-window discriminator (BAK Electronics, Germantown, MD). The spike train was recorded at 1 ms resolution. Only well isolated single units were used for mapping. A Dell 500 MHz Pentium PC was used for stimulus generation and data collection. The eye position monitor was manufactured by CNC Coils (Seattle, WA). The monitor was calibrated before and after each recording session by having the monkey look at dots in the center and four corners of a 5° square on the monitor.

Visual Stimulation

The monkey sat in a dark box with its head rigidly fixed and was given a juice reward for keeping fixation for three seconds within a 1° fixation box. Red/green goggles were used to allow presentation of independent stimuli to each eye (KODAK written filters, cyan #65A and red #25). The amount of leakage through the filters was $<6\%$. The monkey's eye position was recorded every 4 ms for use in the eye-position corrected reverse correlation. All visual stimuli were written using the Scitech MGL Graphics Libarary and were presented at a 60 Hz monitor refresh rate.

Screening for Disparity-Tuned Simple Cells

We screened for disparity-tuned cells with a $3^\circ \times 3^\circ$ dynamic random dot stereogram. The inner ($1^\circ \times 1^\circ$) region of the stereogram modulated between a near (-0.14°) and a far (0.09°) disparity, while the outer region that was fixed at far (0.09°) disparity. The dot density was 30%, and the dot size was 0.03°. The square flashed on for 250 ms and off for 200 ms. Since there were no monocular cues to the disparity of the square, a modulating response necessarily indicated binocular disparity tuning. It is possible that because we used only two disparities, roughly symmetric about zero, our sample was biased against neurons that were symmetrically tuned to zero disparity, but in practice we were able to pick out cells with a variety of disparity-tuning curves. We chose this method of screening in order to go through as many cells as quickly as possible within a recording session.

Receptive Field Mapping

With the exception of one cell, all cells had eccentricities within 3° of the fovea. After a disparity-tuned cell was isolated, we obtained the monocular receptive field map within each eye along the direction perpendicular to the preferred orientation of the cell, which was $<45^\circ$ from vertical for most cells. We first determined the center of the receptive field by flashing a very tiny spot of light on and off, and moving it around until we found the spot that gave optimal excitation. Then, we extended the dot to a bar and rotated it until we found the optimum orientation. To map the cell's receptive field in each eye, we flashed pairs of bars, one red and one cyan, at the refresh rate of the monitor (17 ms) at random locations within a 3° range that extended along the direction perpendicular to the preferred orientation of the cell. The bars were $0.6^\circ \times 0.06^\circ$. We used light bars (red and cyan bars on a black background) to map the ON subregions in the two eyes and dark bars (cyan and red bars on a white background) to map the OFF subregions in the two eyes. Light- and dark-bar maps were obtained in separate blocks. Light stimulus luminance through the filters was 3.7 cd per m^2. We did not use light and dark bars on an intermediate-luminance background because the higher contrast bars gave the strongest, most reproducible, and clearest maps.

We "forward correlated" the resulting spike train to the bar locations by computing the average PSTH (from 0 to 250 ms) in response to stimulation at each location along the one-dimensional mapping range. This generated a "spacetime map" showing the average response of the cell as a function of both space and time. Each map represents at least 6000 spikes. At each spatial location, the PSTH was normalized by its average value between 250 ms and 300 ms to remove effects of inhomogeneous sampling. Light-bar and dark-bar maps were scaled so that the mean firing rate was the same for both, and the maps were smoothed with a pseudo-Gaussian filter (3×3 matrix, sigma $= 0.14^\circ$ in space and 3 ms in time). A cell was classified as simple when either the spatial or the temporal phase shift was $>90^\circ$ between the light- and dark-bar maps.

Spacetime maps were generated both with and without eye position correction (i.e., correcting the bar location for the monkey's eye position so that the receptive field maps would represent the position of the bar on the monkey's retina). However, since we found that eye position correction generally resulted in lower amplitudes and larger receptive field widths, all the results here were computed from uncorrected maps.

Obtaining Disparity-Tuning Curves

We generated two-bar interaction maps by plotting, for each spike and temporal delay, the preceding bar location in the left and right eyes at that delay on the *x* and *y* axis, respectively. The binocular interaction map looks like a cross (Ohzawa et al., 1990; Livingstone and Tsao, 1999). The four arms of the cross represent the monocular receptive field within each eye, while the center of the cross represents the response to binocularly visible bars flashed at different locations and disparities.

Disparity-tuning curves were obtained by superimposing a 45° rotated square (1° side length) on the binocular interaction map, and summing along the iso-disparity lines of this square. For each cell, the same reverse correlation delay was used to obtain the disparity-tuning curve as was used to obtain the monocular receptive field profiles. We repeated this procedure for light- and dark-bar maps and averaged the two maps using the relative number of spikes as a normalization ratio (e.g., if the light-bar map was constructed from half as many spikes as the dark-bar map, then it would be weighted twice as strongly). For a few cells, we used only the contrast giving the most reliable disparity-tuning curve. To obtain error bars, we divided the light- and dark-bar spikes for each cell into two groups, each containing the same number of spikes, and computed the disparity-tuning curve in the above manner sepa-

rately for the two groups. These two independent estimates of the disparity-tuning curve were used to obtain the standard deviation at each disparity.

Since we typically stimulated over a range approximately three times the receptive field width, the binocular interaction maps also contained ample information about purely monocular responses. The monocular response for each eye was obtained by averaging activity under two rectangular regions (0.4° × 1°) positioned over the monocular ends of the arm representing the appropriate eye. The spontaneous response was obtained by averaging activity under four squares (0.4° × 0.4°) positioned over the four corners of the binocular interaction map.

Fitting Monocular Receptive Field Profiles and Disparity-Tuning Curves

We extracted monocular one-dimensional receptive field profiles from the two-dimensional spacetime maps in the following manner: first, we computed the temporal delay at which the maximum response in each eye occurred; then, we averaged the two delays to obtain a single optimum delay; finally, we averaged the spacetime map over the 10 ms surrounding this optimum delay to obtain a one-dimensional receptive field profile.

For each cell, we fit both the left and right eye receptive field profiles to a Gabor function. The formula we used for the Gabor function was: $y = A \cdot \exp(-(x - x_o)^2/2w^2) \cdot \cos(2\pi f(x - x_o) + \phi) + C$. Fitting was done using the Levenberg-Marquardt algorithm, as implement by the MATLAB Statistics Toolbox. The frequency was constrained to be between 0.5 and 2 times the characteristic frequency of the cell (Prince et al., 2002b). The phase was set to a value between −180° and 180°. The characteristic frequency was obtained by performing a discrete Fourier transform of the receptive field profile and taking the frequency at the peak of the power spectrum. No other parameters were formally constrained, though we did check the parameters of each fit manually to ensure sanity (e.g., we confirmed that the variance, w, was always less than the receptive field mapping range). Fitting each eye's receptive field profile to a Gabor yielded an envelope position, x_o, and a phase, ϕ, in each eye. Taking differences between eyes then yielded the position and phase disparity. Actual and predicted disparity-tuning curves were fit to Gabor functions using the same method.

Even though this fitting procedure always yields a particular phase and position difference, it is quite possible that other combinations of phase and position could lead to equally good fits. Therefore, for each cell, we fit the left and right eye receptive fields to four separate curves: (1) Gabor with phase and position parameters free, (2) Gaussian, (3) Gabor with phase parameter free but with the position parameter constrained to be identical in the two eyes, and (4) Gabor with position parameter free but with the phase parameter constrained to be identical in the two eyes. Then sequential F tests were performed to evaluate the significance in fit improvement for Gaussian → Gabor, Gabor with constrained center → Gabor, and Gabor with constrained phase → Gabor. For details, see Supplemental Figure S1 at http://www.neuron.org/cgi/content/full/38/1/103/DC1.

Acknowledgments

We wish to thank David Freeman for all the programming, Tamara Chuprina for technical assistance, Mike Lafratta for machining the hardware, David Hubel, Kevin Duffy, and Christopher Pack for reading the manuscript and making useful comments, and the anonymous reviewers for their valuable contribution. This work was supported by NIH grant EY13135.

Received: July 19, 2001
Revised: January 16, 2003
Accepted: February 26, 2003
Published: April 9, 2003

References

Anderson, B., and Nakayama, K. (1994). Toward a general theory of stereopsis: binocular matching, occluding contours, and fusion. Psychol. Rev. *101*, 414–445.

Anderson, J.S., Lampl, I., Gillespie, D., and Ferster, D. (2000). The contribution of noise to contrast invariance of orientation tuning in cat visual cortex. Science *290*, 1968–1972.

Anzai, A., Ohzawa, I., and Freeman, R.D. (1999a). Neural mechanisms for encoding binocular disparity: receptive field position versus phase. J. Neurophysiol. *82*, 874–890.

Anzai, A., Ohzawa, I., and Freeman, R.D. (1999b). Neural mechanisms for processing binocular information I. Simple cells. J. Neurophysiol. *82*, 891–908.

Anzai, A., Ohzawa, I., and Freeman, R.D. (2001). Joint-encoding of motion and depth by visual cortical neurons: neural basis of the Pulfrich effect. Nat. Neurosci. *4*, 513–518.

Barlow, H., Blakemore, C., and Pettigrew, J. (1967). The neural mechanisms of binocular depth discrimination. J. Physiol. *193*, 327–342.

Burr, D.C., and Ross, J. (1979). How does binocular delay give information about depth? Vision Res. *19*, 523–532.

Conway, B.R. (2001). Spatial structure of cone inputs to color cells in alert macaque primary visual cortex (V-1). J. Neurosci. *21*, 2768–2783.

Conway, B.R., and Livingstone, M.S. (2002). Space-time maps and two-bar interactions of different classes of direction-selective cells in macaque V-1. J. Neurophysiol., in press.

Cumming, B.G., and Parker, A.J. (1997). Responses of primary visual cortical neurons to binocular disparity without depth perception. Nature *389*, 280–283.

Daugman, J.D. (1985). Uncertainty relation for resolution in space, spatial frequency, and orientation optimized by two-dimensional visual cortical filters. J. Opt. Soc. Am. A *2*, 1160–1169.

DeAngelis, G.C. (1993a). Spatiotemporal organization of simple-cell receptive fields in the cat's striate cortex. I. General characteristics and postnatal development. J. Neurophysiol. *69*, 1091–1117.

DeAngelis, G.C. (1993b). Spatiotemporal organization of simple-cell receptive fields in the cat's striate cortex. II. Linearity of temporal and spatial summation. J. Neurophysiol. *69*, 1118–1135.

DeAngelis, G.C., Ohzawa, I., and Freeman, R.D. (1991). Depth is encoded in the visual cortex by a specialized receptive field structure. Nature *352*, 156–159.

Draper, N.R., and Smith, H.S. (1998). Applied Regression Analysis, 3rd Edition (New York: Wiley).

Hubel, D.H., and Wiesel, T.N. (1962). Receptive fields, binocular interaction and functional architecture in the cat's visual cortex. J. Physiol. *160*, 106–154.

Jones, J., and Palmer, L. (1987). An evaluation of the two-dimensional Gabor filter model of simple receptive fields in cat striate cortex. J. Neurophysiol. *58*, 1233–1258.

Julesz, B. (1960). Binocular depth perception of computer-generated patterns. Bell System Technical J. *39*, 1125–1162.

Livingstone, M.S. (1998). Mechanisms of direction selectivity in macaque V1. Neuron *20*, 509–526.

Livingstone, M.S., and Tsao, D.Y. (1999). Receptive fields of disparity-selective neurons in macaque striate cortex. Nat. Neurosci. *2*, 825–832.

Marcelja, S. (1980). Mathematical description of the responses of simple cortical cells. J. Opt. Soc. Am. *70*, 1297–1300.

Maske, R., Yamane, S., and Bishop, P.O. (1984). Binocular simple cells for local stereopsis: comparison of receptive field organization for the two eyes. Vision Res. *24*, 1921–1929.

McLean, J., and Palmer, L. (1989). Contribution of linear spatiotemporal receptive field structure to velocity selectivity of simple cells in area 17 of cat. Vision Res. *29*, 675–679.

Movshon, J.A., Thomson, I.D., and Tolhurst, D.J. (1978). Spatial summation in the receptive fields of simple cells in the cat's striate cortex. J. Physiol. *283*, 53–77.

Nakayama, K., and Shimojo, S. (1990). Da Vinci stereopsis: depth and occluding contours from unpaired image points. Vision Res. *30*, 1811–1825.

Ohzawa, I., Angelis, G.C., and Freeman, R.D. (1990). Stereoscopic

depth discrimination in the visual cortex: neurons ideally suited as disparity detectors. Science *249*, 1037–1041.

Ohzawa, I., DeAngelis, G.C., and Freeman, R.D. (1996). Encoding of binocular disparity by simple cells in the cat's visual cortex. J. Neurophysiol. *75*, 1779–1805.

Pettigrew, J. (1965). Binocular Interaction on Single Units of the Striate Cortex of the Cat (Sydney, Australia: University of Sydney).

Poggio, G.F. (1990). Cortical mechanisms of stereopsis studied with dynamic random-dot stereograms. Cold Spring Harb. Symp. Quant. Biol. *55*, 749–758.

Poggio, G.F., and Fischer, B. (1977). Binocular interaction and depth sensitivity of striate and prestriate cortex of behaving rhesus monkey. J. Neurophysiol. *40*, 1392–1405.

Poggio, G., and Poggio, T. (1984). The analysis of stereopsis. Annu. Rev. Neurosci. *7*, 379–412.

Poggio, G., Gonzalez, F., and Krause, F. (1988). Stereoscopic mechanisms in monkey visual cortex: binocular correlation and disparity selectivity. J. Neurosci. *8*, 4531–4550.

Press, W.B., Teukolsky, S., Vetterling, W., and Flannery, B. (1992). Numerical Recipes in C: The Art of Scientific Computing (Cambridge, UK: Cambridge University Press).

Prince, S.J.D., Cumming, B.G., and Parker, A.J. (2002a). Range and mechanism of encoding of horizontal disparity in macaque V1. J. Neurophysiol. *87*, 209–221.

Prince, S.J.D., Pointon, A.D., Cumming, B.G., and Parker, A.J. (2002b). Quantitative analysis of the responses of V1 neurons to horizontal disparity in dynamic random-dot stereograms. J. Neurophysiol. *87*, 191–208.

Qian, N. (1997). Binocular disparity and the perception of depth. Neuron *18*, 359–368.

Qian, N., and Andersen, R.A. (1997). A physiological model for motion-stereo integration and a unified explanation of Pulfrich-like phenomena. Vision Res. *37*, 1683–1698.

Reid, R.C., Soodak, R.E., and Shapley, R.M. (1991). Direction selectivity and spatiotemporal structure of receptive fields of simple cells in cat striate cortex. J. Neurophysiol. *66*, 505–529.

Shimojo, S., Silverman, G.H., and Nakayama, K. (1988). An occlusion-related mechanism of depth perception based on motion and interocular sequence. Nature *333*, 265–268.

Zar, J.H. (1999). Biostatistical Analysis, 4th Edition (New Jersey: Prentice Hall).